Monthly Notices
of the
ROYAL ASTRONOMICAL SOCIETY

MNRAS **460,** 3447–3457 (2016)
Advance Access publication 2016 May 12

doi:10.1093/mnras/stw1122

Optical photometry and spectroscopy of the 1987A-like supernova 2009mw

K. Takáts,[1,2★] G. Pignata,[2,1] M. Bersten,[3,4,5] M. L. Rojas Kaufmann,[3] J. P. Anderson,[6] G. Folatelli,[3,4,5] M. Hamuy,[7,1] M. Stritzinger,[8] J. B. Haislip,[9] A. P. LaCluyze,[9] J. P. Moore[9] and D. Reichart[9]

[1]*Millennium Institute of Astrophysics,Vicuña Mackenna 4860, 7820436 Macul, Santiago, Chile*
[2]*Departamento de Ciencias Fisicas, Universidad Andres Bello, Avda. Republica 252, Santiago, Chile*
[3]*Facultad de Ciencias Astronómicas y Geofísicas, Universidad Nacional de La Plata (UNLP), Paseo del Bosque S/N, B1900FWA, La Plata, Argentina*
[4]*Instituto de Astrofísica La Plata, IALP, CCT-CONICET-UNLP, Paseo del Bosque s/n, B1900FWA, La Plata, Argentina*
[5]*Kavli Institute for the Physics and Mathematics of the Universe (WPI), The University of Tokyo, Kashiwa, Chiba 277-8583, Japan*
[6]*European Southern Observatory, Alonso de Córdova 3107, Casilla 19001, Santiago, Chile*
[7]*Departamento de Astronomía, Universidad de Chile, Casilla 36-D, Santiago, Chile*
[8]*Department of Physics and Astronomy, Aarhus University, Ny Munkegade, DK-8000 Aarhus C, Denmark*
[9]*University of North Carolina at Chapel Hill, Campus Box 3255, Chapel Hill, NC 27599-3255, USA*

Accepted 2016 May 10. Received 2016 May 9; in original form 2016 January 20

ABSTRACT

We present optical photometric and spectroscopic observations of the 1987A-like supernova (SN) 2009mw. Our *BVRI* and $g'r'i'z'$ photometry covers 167 d of evolution, including the rise to the light-curve maximum, and ends just after the beginning of the linear tail phase. We compare the observational properties of SN 2009mw with those of other SNe belonging to the same subgroup and find that it shows similarities to several objects. The physical parameters of the progenitor and the SN are estimated through hydrodynamical modelling, and yield an explosion energy of 1 foe, a pre-SN mass of 19 $M_\odot$, a progenitor radius of 30 $R_\odot$ and a ^{56}Ni mass of 0.062 $M_\odot$. These values indicate that the progenitor of SN 2009mw was a blue supergiant star, similar to the progenitor of SN 1987A. We examine the host environment of SN 2009mw and find that it emerged from a population with a slightly subsolar metallicty.

Key words: supernovae: general – supernovae: individual: SN 1987A – supernovae: individual: SN 2009mw.

1 INTRODUCTION

The explosion of supernova (SN) 1987A in the Large Magellanic Cloud was a unique event that has improved our understanding of the evolution of massive stars immeasurably. It is the most studied SN ever, and is the subject of a vast amount of published literature. It was also a high-impact event in the sense that very few similar SNe have been observed to date. SNe of this type involve core-collapse and have spectra akin to those of the very common SNe II-P. However, while both models and observations have found that SNe II-P emerge from red supergiant (RSG) stars, the progenitor of SN 1987A was a blue supergiant (BSG, see Arnett et al. 1989, and references therein).

1987A-like SNe are intrinsically rare: Pastorello et al. (2012) estimated that they represent about 1–3 per cent of all core-collapse SNe in a volume-limited sample. In fact, after SN 1987A the astronomical community had to wait 11 years for the discovery of the next similar event, SN 1998A (Pastorello et al. 2005). Since then a few more objects have been studied. Kleiser et al. (2011) published observations of SNe 2000cb and 2005ci, although they note that SN 2000cb does not match the characteristics of either SNe II-P or SN 1987A: its *B*-band light curve is more similar to that of SNe II-P, while in the redder bands it shows the slow-rising light curve of 1987A-like SNe, and therefore its classification as a 1987A-like object is questionable. Taddia et al. (2012) presented data on SNe 2006V and 2006au, while Pastorello et al. (2012) published data on SN 2009E, all of which are well-observed examples of this subgroup. Pastorello et al. (2012) compiled the sample of 1987A-like SNe known to date: 11 objects in total, including SN 1987A and SN 2000cb. Arcavi (2012) showed from the light curves of SNe 2004ek, 2004em and 2005dp that these objects might also belong to this subgroup. Taddia et al. (2016) analysed the data of SNe 2004ek, 2004em, 2005ci and 2005dp, and added to the sample

★ E-mail: ktakats@gmail.com

PTF09gpn and PTF12kso. The light curve of SN 2004ek resembles that of SN 2000cb. Kelly et al. (2015) classified SN Refsdal as a luminous 1987A-like SN. In summary, the entire available sample of 1987A-like SNe consists of a maximum of 17 objects, with only a handful of them having well-sampled, multiband light curves and spectroscopic observations.

In this paper we report on the observations of SN 2009mw, a member of the group of 1987A-like objects. SN 2009mw was discovered on 2009 December 23.30 UT in ESO 499-G005 by the Chilean Supernova Search (CHASE, Pignata et al. 2009) project, and was classified as a Type II-P SN on December 25.2 UT (Maza et al. 2009). The classification spectrum suggested a normal SN II-P about a month after the explosion; however, the subsequent photometric follow-up revealed a light curve similar to that of SN 1987A.

This paper is organized as follows. In Section 2 we present the photometric data and light-curve analysis. In Section 3 we provide the spectroscopic follow-up data and compare it with those for other 1987A-like SNe. We estimate the physical parameters of the progenitor and the explosion of SN 2009mw using hydrodynamical modelling in Section 4, and analyse the host environment in Section 5. Finally, the results are summarized and discussed in Section 6.

2 PHOTOMETRY

Optical photometric observations of SN 2009mw were obtained with the PROMPT Telescopes in *BVRI*, $g'r'i'z'$, and open filters. The data reduction was carried out using standard IRAF[1] tasks. After the basic reduction steps (bias-subtraction, overscan-correction, flat-fielding), the photometric measurements of the SN were performed using the point-spread function (PSF) fitting technique. We calibrated the photometry by observing standard fields (Landolt 1992; Landolt & Uomoto 2007; Smith et al. 2002) on photometric nights. With the help of these images, magnitudes for a local sequence of stars (Fig. 1, Table 1) in the SN field were determined and used to calibrate the SN measurements (Fig. 2, Table 2). Some of our observations were taken without a filter. Because the effective wavelength without a filter and shaped by the CCD quantum efficiency is close to the effective wavelength of the *R* band, we decided to calibrate the unfiltered instrumental magnitudes to this band. In order to compute the transformation we used a colour term estimated by observing Landolt standard stars without a filter; that is, with the same setup as used for the SN observations.

Our observations lasted for about 167 d after discovery, covering the evolution around the maximum and ending just after the tail phase started. By fitting a low-order polynomial around the maximum, we determined that the *B*-band maximum occurred 71 d after the discovery epoch, namely on MJD 55258.8 ± 0.4, with an apparent magnitude of $m_B = 18.99 \pm 0.02$ mag.

In Fig. 3 we compare the $BVRr'Ii'$ light-curve shapes of several 1987A-like SNe with those of SN 2009mw. Some relevant parameters of the SNe that we use for comparison throughout the paper can be found in Table 3. In Fig. 3, the light curves of the comparison SNe are shifted vertically to match the peak magnitudes of SN 2009mw. This figure shows that the light-curve shapes of the different objects are quite similar; only those of SN 2000cb differ significantly, showing flatter curves in *VRI* bands and missing the broad, late maximum of the *B*-band curve entirely.

[1] IRAF is distributed by the National Optical Astronomy Observatories, which are operated by the Association of Universities for Research in Astronomy, Inc., under cooperative agreement with the National Science Foundation.

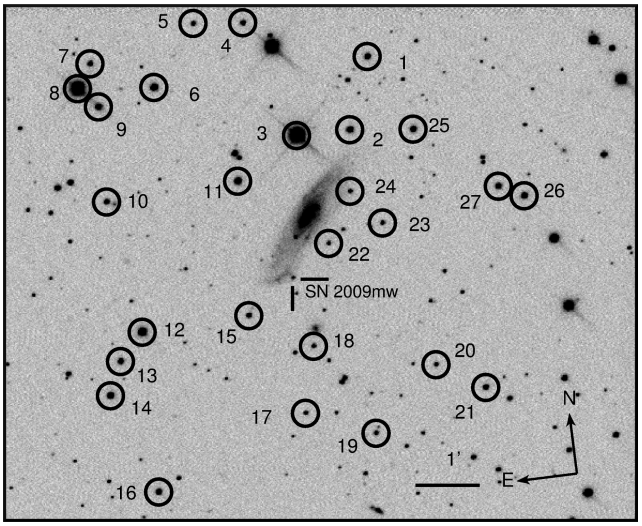

Figure 1. The field of SN 2009mw taken with the PROMPT5 telescope in the *R* band. The local sequence of stars used for the photometric calibration is marked with numbers. Their magnitudes can be found in Table 1.

Because we do not have non-detections to constrain the explosion epoch of SN 2009mw, we have to rely on comparisons with other similar objects. In the small sample of this subgroup, the only SN with a well-known explosion epoch is SN 1987A. The *B*-maximum of this object occurred 82.2 ± 1.1 d after the explosion. Another SN with some constraints on the explosion epoch is SN 2009E (Pastorello et al. 2012), which exploded 86.5 ± 6.8 d before the *B*-maximum. This value is similar to that of SN 1987A, but with higher uncertainties. We determined the explosion epoch of SN 2009mw by adopting the weighted mean of the two values, 84.3 ± 3.5 d, leading to the explosion epoch MJD 55174.5 (2009 December 9.5 UT), 14 d before discovery.

2.1 Reddening and colour curves

The galactic reddening in the direction of SN 2009mw is $E(B-V)_{\rm MW} = 0.054 \pm 0.001$ mag (Schlafly & Finkbeiner 2011). In the spectra (Section 3) there are no visible Na I D absorption lines, the usual tracers of host galaxy extinction. We therefore assume that the host galaxy extinction component is negligible and adopt the galactic component as the total reddening towards the SN.

Fig. 4 shows the $(B-V)_0$, $(V-R)_0$ and $(V-I)_0$ colours corrected with $E(B-V) = 0.054$ mag. Because the epochs of the *B*-band photometry differ from the others, we interpolated the *V*-band light curve to the epochs of the *B*-band observations in order to calculate the $(B-V)_0$ colour curve. In Fig. 4 we also compare the colours with those of other 1987A-like objects. The reddening values of these SNe can be found in Table 3. In the case of SNe 2006V and 2006au, *ri*-band magnitudes are available instead of *RI*-band observations (Taddia et al. 2012). We included these objects in the colour comparison by transforming the *ri* magnitudes to the Johnson system using the formulae of Jordi, Grebel & Ammon (2006). Because these equations were calibrated for stars, first we tested them by converting the $r'i'$ magnitudes of SN 2009mw to *RI* magnitudes and comparing the results with measured values. We found that they agree within 1σ. Encouraged by this, we converted

Table 1. *BVRI* and $g'r'i'z'$ magnitudes of the local sequence of stars used for the photometric calibration.

	α_{2000}	δ_{2000}	Dec. [mag]	B [mag]	V [mag]	R [mag]	I [mag]	g' [mag]	r' [mag]	i' [mag]	z' [mag]
1	09:47:07.942	−24:48:00.74	16.511 (0.025)	15.546 (0.035)	15.044 (0.043)	14.508 (0.047)	16.003 (0.013)	15.273 (0.029)	14.979 (0.017)	14.815 (0.004)	
2	09:47:09.775	−24:49:06.95	15.480 (0.019)	15.025 (0.026)	14.745 (0.043)	14.456 (0.043)	15.246 (0.029)	14.936 (0.035)	14.847 (0.014)	14.819 (0.009)	
3	09:47:13.471	−24:49:06.13	13.053 (0.032)	11.575 (0.021)			12.256 (0.020)	11.081 (0.032)	10.571 (0.089)	10.177 (0.012)	
4	09:47:16.186	−24:47:14.58	16.741 (0.035)	16.176 (0.027)	15.805 (0.053)	15.438 (0.026)	16.418 (0.024)	16.029 (0.030)	15.863 (0.026)	15.778 (0.017)	
5	09:47:19.600	−24:47:09.37	17.502 (0.050)	16.793 (0.016)	16.391 (0.046)	15.978 (0.039)	17.122 (0.033)	16.601 (0.043)	16.373 (0.049)	16.327 (0.024)	
6	09:47:22.843	−24:48:04.46	14.843 (0.018)	14.402 (0.030)	14.129 (0.050)	13.831 (0.031)	14.610 (0.022)	14.316 (0.042)	14.217 (0.018)	14.196 (0.013)	
7	09:47:27.022	−24:47:34.86	16.733 (0.034)	15.989 (0.022)	15.585 (0.068)	15.190 (0.032)	16.321 (0.026)	15.802 (0.036)	15.606 (0.018)	15.518 (0.011)	
8	09:47:28.092	−24:47:56.56	12.471 (0.018)	11.714 (0.032)	11.282 (0.046)	10.836 (0.028)	12.056 (0.024)	11.503 (0.034)	11.268 (0.020)	11.157 (0.011)	
9	09:47:26.815	−24:48:16.03	15.809 (0.023)	15.203 (0.031)	14.872 (0.046)	14.490 (0.047)	15.486 (0.021)	15.066 (0.034)	14.905 (0.022)	14.832 (0.007)	
10	09:47:27.083	−24:49:45.66	17.515 (0.033)	16.317 (0.051)	15.613 (0.063)	14.972 (0.041)	16.906 (0.015)	15.883 (0.038)	15.462 (0.028)	15.223 (0.004)	
11	09:47:17.905	−24:49:41.74	15.496 (0.017)	14.754 (0.032)	14.337 (0.043)	13.949 (0.035)	15.124 (0.021)	14.550 (0.034)	14.375 (0.013)	14.289 (0.008)	
12	09:47:25.767	−24:51:51.35	15.251 (0.014)	14.143 (0.034)	13.483 (0.052)	12.909 (0.039)	14.695 (0.013)	13.746 (0.031)	13.382 (0.019)	13.194 (0.019)	
13	09:47:27.512	−24:52:16.16	16.123 (0.029)	15.521 (0.025)	15.208 (0.056)	14.843 (0.047)	15.802 (0.012)	15.400 (0.027)	15.260 (0.021)	15.210 (0.020)	
14	09:47:28.495	−24:52:46.94	15.623 (0.020)	14.947 (0.030)	14.603 (0.045)	14.229 (0.043)	15.260 (0.011)	14.804 (0.031)	14.645 (0.019)	14.578 (0.006)	
15	09:47:18.305	−24:51:48.53	17.077 (0.039)	16.337 (0.023)	15.949 (0.048)	15.536 (0.051)	16.672 (0.015)	16.176 (0.043)	15.987 (0.022)	15.871 (0.041)	
16	09:47:26.020	−24:54:22.44	16.790 (0.034)	15.719 (0.027)	15.127 (0.067)	14.541 (0.038)	16.248 (0.006)	15.383 (0.046)	15.024 (0.042)	14.809 (0.010)	
17	09:47:15.264	−24:53:26.23	17.343 (0.036)	16.978 (0.061)	16.798 (0.046)	16.507 (0.039)	17.123 (0.012)	16.957 (0.037)	16.895 (0.021)	16.922 (0.058)	
18	09:47:14.135	−24:52:24.69	17.767 (0.050)	17.128 (0.038)	16.767 (0.045)	16.411 (0.059)	17.453 (0.045)	16.991 (0.029)	16.834 (0.018)	16.736 (0.014)	
19	09:47:10.597	−24:53:53.18	17.627 (0.059)	16.872 (0.028)	16.473 (0.059)	16.056 (0.064)	17.217 (0.025)	16.688 (0.029)	16.478 (0.011)	16.399 (0.021)	
20	09:47:05.893	−24:52:56.25	18.063 (0.129)	17.122 (0.039)	16.651 (0.039)	16.167 (0.050)	17.563 (0.039)	16.873 (0.012)	16.632 (0.026)	16.476 (0.042)	
21	09:47:02.678	−24:53:23.33	16.929 (0.009)	16.035 (0.021)	15.495 (0.063)	14.967 (0.033)	16.461 (0.011)	15.737 (0.034)	15.424 (0.020)	15.251 (0.021)	
22	09:47:12.206	−24:50:50.50	17.757 (0.037)	17.016 (0.076)	16.647 (0.020)	16.213 (0.033)	17.382 (0.025)	16.851 (0.020)	16.682 (0.024)	16.553 (0.051)	
23	09:47:08.336	−24:50:37.78	17.774 (0.058)	16.992 (0.062)	16.580 (0.082)	16.149 (0.035)	17.356 (0.014)	16.804 (0.024)	16.592 (0.035)	16.472 (0.033)	
24	09:47:10.292	−24:50:04.39	17.922 (0.084)	17.261 (0.035)	16.893 (0.046)	16.489 (0.043)	17.596 (0.055)	17.099 (0.041)	16.896 (0.025)	16.794 (0.056)	
25	09:47:05.428	−24:49:13.87	15.829 (0.020)	15.253 (0.032)	14.927 (0.046)	14.588 (0.046)	15.525 (0.028)	15.119 (0.033)	15.003 (0.016)	14.954 (0.020)	
26	09:46:58.392	−24:50:29.08	15.694 (0.026)	15.088 (0.029)	14.751 (0.048)	14.394 (0.040)	15.370 (0.037)	14.944 (0.035)	14.800 (0.019)	14.741 (0.009)	
27	09:47:00.077	−24:50:17.13	16.764 (0.028)	15.718 (0.030)	15.072 (0.046)	14.507 (0.039)	16.228 (0.031)	15.318 (0.038)	14.979 (0.017)	14.797 (0.023)	

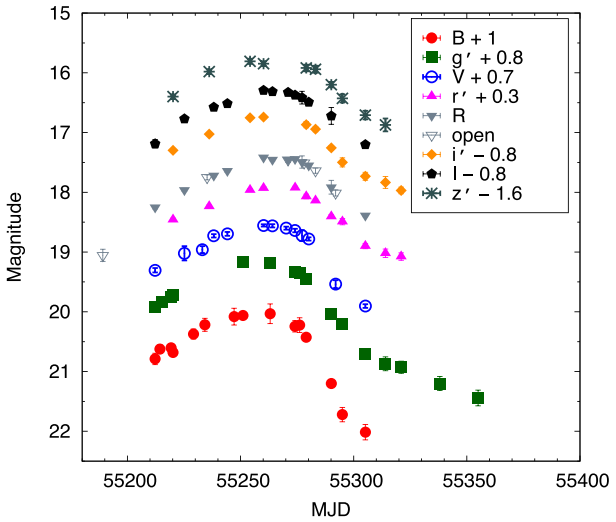

Figure 2. The *BVRI* and $g'r'i'z'$ light curves of SN 2009mw.

the *ri* magnitudes of SNe 2006V and 2006au to the *RI* bands and used these values for the colour comparison.

Fig. 4 shows the colour comparison between SN 2009mw and the other SNe in our sample. SN 1987A has redder colours during its pre-maximum evolution than most of the sample, but this difference seems to disappear at later times. The $B - V$ colour of SN 2000cb reddens steadily during the first ∼80 d of evolution. There is some scatter among the rest of the SNe in the $(B - V)_0$ colour, while in the other two colours these objects are similar. The $(V - R)_0$ and $(V - I)_0$ colours of all the SNe, except those of SN 2000cb, are almost constant until about 110–120 d after explosion (∼30 d after maximum), and then the SNe become suddenly redder. This change probably marks the end of the recombination (plateau) phase. At phases later than 120 d after explosion, the $(V - I)_0$ colour of SN 2009E is redder than that of the other SNe, although not all objects have such late observations available.

2.2 Distance and bolometric light curve

There are several distance measurements in the literature for the host galaxy of SN 2009mw, ESO 499-G005, all obtained using the Tully–Fisher (TF) method. Willick et al. (1997) obtained a Malmquist-corrected TF distance of 44.69 ± 8.5 Mpc. Theureau et al. (2007) used the TF method in the *JHK* band and obtained an average distance of 57.93 ± 10.6 Mpc. Springob et al. (2009) found the Malquist-corrected TF distance to be 44.29 ± 8.13 Mpc. The redshift distance is 57 ± 4 Mpc.[2] In this paper we adopt the weighted mean of these distances, $D = 50.95 \pm 4.07$ Mpc (distance modulus $\mu = 33.54 \pm 0.17$ mag).

The *B*-band peak absolute magnitude of SN 2009mw calculated using the obtained distance is $M_{B,\max} = -14.77 \pm 0.17$ mag. This value is among the lowest in our sample of 1987A-like SNe (Table 3); it is similar to that of SN 1987A and only slightly higher than that of SN 2009E.

Fig. 5 compares the *BVRI* quasi-bolometric luminosities of 1987A-like SNe with that of SN 2009mw. We used the same method for all of the SNe to calculate these luminosities, by converting the *BVRI* magnitudes to fluxes and integrating them using Simpson's rule. The distances of the SNe used for comparison can be found in Table 3. The luminosity of SN 2009mw is similar to that of SN 2009E and lower than that of SN 1987A.

[2] NED; http://ned.ipac.caltech.edu/.

3 SPECTROSCOPY

Four optical spectra were taken of SN 2009mw with the 8.1-m Gemini South Telescope (+GMOS), the 4.1-m Southern Astrophysical Research Telescope (SOAR+Goodman) and the 2.5-m Irénée du Pont telescope (+WFCCD) (see Table 4). The reduction, extraction and calibration of the spectra were carried out using standard IRAF tasks. In the case of the Gemini-S data, we used the tasks in the GEMINI package in IRAF. Note that the wavelength calibration of the first spectrum is somewhat uncertain, because we had to use the night sky lines for calibration. The reduced spectra are shown in Fig. 6.

The spectra show features that are typically present in SNe II-P during the recombination phase, such as the H I Balmer series, Na II, Ca II, Ba II, Fe II, Sc II and Ti II (Fig. 7). During the observed period the same features remain present, while the Na I and H I lines strengthen significantly.

In Fig. 7 we compare the spectra of SN 2009mw with those of other 1987A-like SNe at similar phases. The spectra of SN 2009mw are the most similar to those of SNe 1998A and 2006au, mainly because of their more prevalent Hβ absorption features and very weak Ba II lines. The Ba II features are quite strong in the spectra of SNe 1987A and 2009E. Strong Ba II features often appear in the spectra of subluminous SNe II-P, and their appearance is usually explained by invoking temperature effects (see e.g. Turatto et al. 1998; Pastorello et al. 2012; Takáts et al. 2014).

In order to compare quantitatively the strength of some of the features in different SNe, we measured the pseudo-equivalent widths (pEWs) of the absorption components of Hα, Hβ, Fe II λ5169 and Ba II λ6142 features. In Fig. 8 we compare these values. The pEWs of Hα show a large scatter among the different SNe, while the pEWs of Hβ seem to split into two groups at phase 40 d after explosion, with SNe 2009mw, 1998A, 2000cb and 2006au having pEWs greater than 30 Å, while the pEW values of SNe 1987A, 2006V and 2009E are significantly smaller, lower than 10 Å at this epoch. We can detect a similar duality in the pEWs of Ba II: in this case SNe 1987A and 2009E have larger values than the rest. The pEWs of the H I lines of SN 1987A show an interesting behaviour: the pEWs of both Hα and Hβ increase rapidly after explosion, reaching their peak at 19 and 8 d after explosion, respectively, and then decrease rapidly. Lyubimkov (1991) analysed this behaviour and concluded that it is caused by the temperature evolution and the difference in density between the layers that produce Hα and Hβ. In our sample, SNe 2000cb and 2006au seem to show similar behaviour, although they are less well sampled.

The pEWs of Hα and Hβ measured from the first spectrum of SN 2009mw indicate the lack of the sharp peak of pEWs in the case of this SN; or, possibly, the maximum of the pEWs of the Balmer lines are earlier than in the case of SN 1987A. We measured the temperatures of the SNe in our sample by fitting blackbody curves to their spectra (Fig. 9). The temperature of SN 1987A shows a rapid decrease until about 20 d after explosion. The early-time temperatures of SN 2000cb are lower and the decrease is less steep, while for the rest of the SNe we do not have sufficient observations to compare their behaviours at this phase. At a time of 20 d after the explosion, all the SNe in our sample have significantly higher temperatures than SN 1987A, which is reflected in the colour curves (Fig. 4).

Table 2. *BVRI* and $g'r'i'z'$ magnitudes of SN 2009mw, obtained with the PROMPT telescopes.

Date	MJD	B [mag]	V [mag]	R [mag]	I [mag]	g' [mag]	r' [mag]	i' [mag]	z' [mag]
2009/12/23[a]	55188.3			19.124 (0.079)					
2009/12/24[a]	55189.1			19.055 (0.102)					
2009/12/27[a]	55192.2			18.893 (0.065)					
2010/01/10[a]	55206.3			18.457 (0.057)					
2010/01/11[a]	55207.8			18.380 (0.052)					
2010/01/15[a]	55211.2			18.226 (0.044)					
2010/01/16	55212.2	19.789 (0.095)	18.605 (0.037)	18.250 (0.030)	17.988 (0.043)	19.121 (0.070)			
2010/01/18	55214.4	19.625 (0.072)							
2010/01/19	55215.2					19.042 (0.058)			
2010/01/23	55219.3	19.604 (0.061)				18.950 (0.059)			
2010/01/24	55220.2	19.681 (0.062)				18.921 (0.050)	18.159 (0.026)	18.097 (0.026)	17.999 (0.0369)
2010/01/29	55225.2		18.321 (0.034)	17.960 (0.028)	17.571 (0.027)				
2010/02/02	55229.2	19.372 (0.084)							
2010/02/06	55233.1		18.260 (0.058)						
2010/02/07	55234.2	19.218 (0.048)							
2010/02/08[a]	55235.2			17.750 (0.042)					
2010/02/09	55236.1						17.935 (0.023)	17.826 (0.027)	17.581 (0.038)
2010/02/11	55238.1		18.028 (0.029)	17.718 (0.024)					
2010/02/17	55244.1		17.996 (0.032)	17.641 (0.026)	17.315 (0.021)				
2010/02/20	55247.1	19.081 (0.056)							
2010/02/24	55251.1	19.064 (0.030)				18.373 (0.021)			
2010/02/27	55254.2						17.662 (0.027)	17.553 (0.030)	17.407 (0.042)
2010/03/05	55260.2		17.854 (0.019)	17.416 (0.019)	17.093 (0.022)		17.630 (0.026)	17.541 (0.029)	17.447 (0.037)
2010/03/08	55263.1	19.033 (0.044)				18.382 (0.033)			
2010/03/09	55264.1		17.861 (0.028)	17.453 (0.024)	17.114 (0.020)				
2010/03/15	55270.2		17.900 (0.025)						
2010/03/16[a]	55271.0			17.455 (0.039)					
2010/03/16	55271.1			17.456 (0.021)	17.127 (0.023)				
2010/03/19	55274.1	19.243 (0.046)	17.94. (0.029)	17.441 (0.027)	17.173 (0.022)	18.537 (0.039)	17.624 (0.026)		
2010/03/21	55276.1	19.223 (0.065)				18.555 (0.038)			
2010/03/22	55277.1		18.025 (0.040)	17.493 (0.023)	17.216 (0.039)				
2010/03/23[a]	55278.1			17.506 (0.051)					
2010/03/24	55279.0	19.425 (0.049)				18.645 (0.036)	17.770 (0.039)	17.668 (0.051)	17.519 (0.055)
2010/03/25	55280.1		18.081 (0.027)	17.548 (0.022)	17.291 (0.020)				
2010/03/28[a]	55283.1			17.638 (0.044)			17.839 (0.025)	17.743 (0.045)	17.541 (0.059)
2010/04/04	55290.1	20.201 (0.035)		17.915 (0.115)	17.522 (0.140)	19.234 (0.033)	18.105 (0.032)	18.056 (0.037)	17.799 (0.044)
2010/04/06	55292.0		18.838 (0.066)						
2010/04/06[a]	55292.0			18.011 (0.052)					
2010/04/09	55295.0	20.721 (0.129)				19.410 (0.068)	18.191 (0.053)	18.299 (0.076)	18.028 (0.069)
2010/04/19	55305.1	21.015 (0.129)	19.204 (0.049)	18.387 (0.032)	18.001 (0.033)	19.906 (0.078)	18.600 (0.044)	18.532 (0.066)	18.308 (0.072)
2010/04/21	55307.0		19.112 (0.086)		18.045 (0.052)				
2010/04/27	55313.0		19.330 (0.053)	18.562 (0.035)	18.158 (0.039)				
2010/04/28	55314.0					20.070 (0.116)	18.721 (0.071)	18.635 (0.099)	18.472 (0.108)
2010/05/05	55321.0					20.128 (0.101)	18.776 (0.062)	18.769 (0.055)	
2010/05/22	55338.0					20.400 (0.116)			
2010/06/04	55351.0		19.754 (0.059)						
2010/06/08	55355.0			18.876 (0.042)		20.643 (0.131)			

[a]Open filter.

The pEWs of the Fe II lines show some scatter at early phases but are quite similar for all the SNe except 2009E at around 70 d after explosion. Anderson, Gutiérrez & Dessart (2016) found a correlation between the pEW of the Fe II features and the oxygen abundance of the host environment of SNe II. Assuming that this correlation exists for 1987A-like SNe, similar pEWs of Fe II lines would indicate that the objects in our sample emerged from similar environments (see also Section 5). Fig. 8 also indicates that SN 2009E is quite peculiar, because the pEWs of almost all of its lines are low, except that of the Ba II feature, which is significantly higher than that in most of the other SNe.

We measured the Doppler velocity of several lines in the spectra of SN 2009mw, as well as in those of the other 1987A-like SNe. Fig. 10 compares the velocities measured from Hα, Hβ and Fe II λ5169. These velocities show little difference, although during the first 10 d of evolution we have data from only SNe 1987A and 2000cb, and this is the period when the velocity changes more rapidly. At later phases, the velocity curves are quite flat. SN 2009E has lower velocities than the others in this sample, while SN 2009mw has values similar to those of SNe 1998A and 2006au.

4 PHYSICAL PARAMETERS

A comparison of the observed parameters of a SN with those derived from semi-analytical and hydrodynamical modelling is a frequently used technique to estimate the physical properties of the progenitor and the explosion. Here we use a one-dimensional Lagrangian local thermodynamic equilibrium (LTE) radiation hydrodynamic code (Bersten, Benvenuto & Hamuy 2011) for this purpose. We adopted double polytropic models as initial conditions for our simulations. These parametric models preserve the typical density structure of blue supergiant (BSG) stars, which are commonly assumed to be the progenitors of 1987A-like SNe. While pre-SN models calculated from stellar evolution have

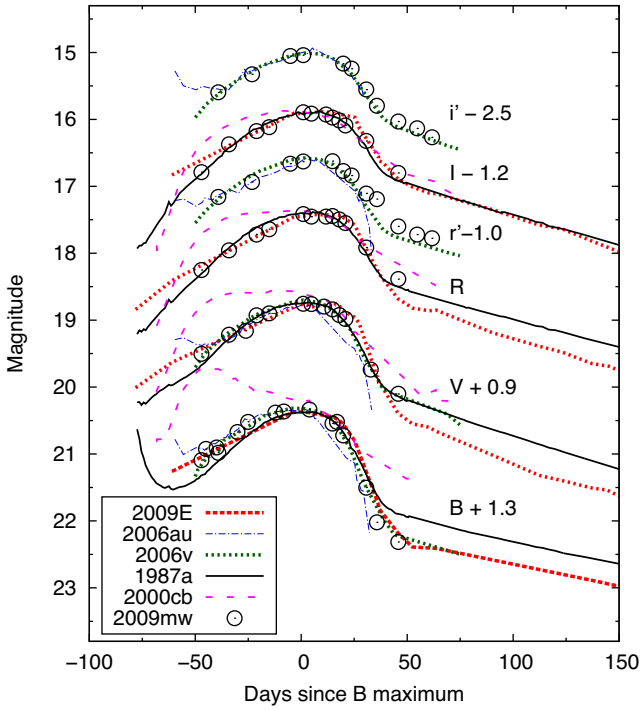

Figure 3. Comparison of the shapes of the $BVRr'Ii'$ light curves for a selected sample of 1987A-like SNe with those of SN 2009mw. The light curves of the comparison SNe were shifted vertically to match the magnitudes of SN 2009mw at maximum, and horizontally to match the epoch of the maximum. Because the *B*-band light curve of SN 2000cb does not show a broad delayed maximum like the others, it was shifted (somewhat arbitrarily) by 76 d relative to the explosion date for the sake of the comparison.

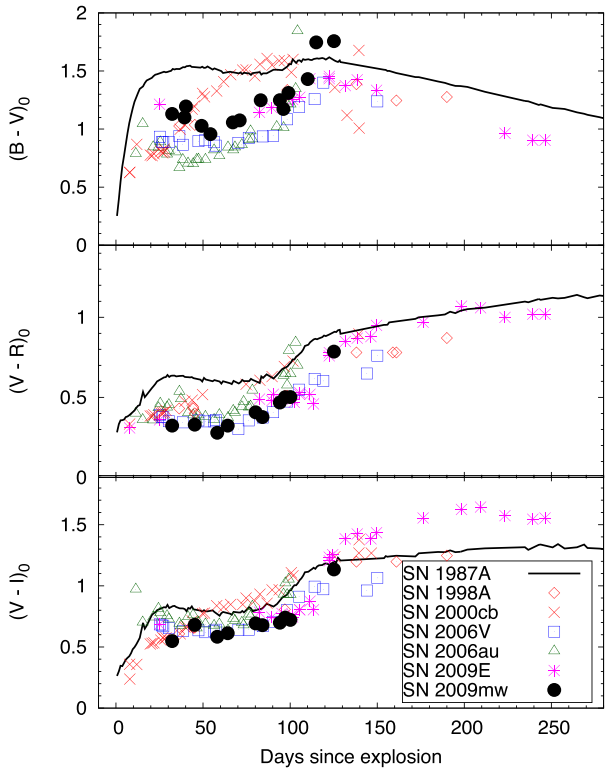

Figure 4. The reddening-corrected $(B-V)_0$, $(V-R)_0$ and $(V-I)_0$ colour curves of SN 2009mw compared with the colour curves of other 1987A-like SNe. Note that the *RI* magnitudes of SNe 2006V and 2006au were transformed from their *ri* bands (see text).

a clearer physical basis, especially if we are to connect the pre-SN mass with the mass of the star on the main sequence, we do not have access to a set of such models for BSGs. We note that in double polytropic models the pre-SN mass and radius are assumed to be independent parameters, to be determined based on a comparison with the observations. The explosion itself was simulated by injecting a certain amount of energy near the centre of the progenitor object. We simultaneously modelled the velocity curve, using the velocities determined from the Doppler shift of the Fe II λ5169 line, and the bolometric luminosity curve resulting from the degeneracy between the progenitor mass and expansion velocities.

Because we do not have either UV or NIR data to calculate the bolometric luminosity directly, we followed the example of Pastorello et al. (2012), by assuming that the bolometric correction is identical for SNe 1987A and 2009mw. We calculated $L_{BVRI,87A}$ using the same method as for SN 2009mw (Section 2.2), while the bolometric luminosity curve was adopted from the literature (Catchpole et al. 1987, 1988). The determined bolometric correction for SN 1987A allowed us to calculate the $L_{\rm bol,09mw}$ curve, which is shown in Fig. 11.

In the same figure, we also present the best-fitting model, which corresponds to a progenitor radius of $30\,{\rm R}_\odot$, an explosion energy of 1 foe, a ^{56}Ni mass of $0.062 M_\odot$, and a pre-SN mass of $19\,{\rm M}_\odot$, assuming that a compact remnant of $1.5\,{\rm M}_\odot$ was formed during the explosion (model M19R30E1Ni062). In order to find this model, several calculations with different masses, radii, energies and radioactive materials were performed. Fortunately, each parameter affects the resulting light curve in a particular way. Even if there is degeneracy between the explosion energy and the pre-SN mass,

Table 3. The explosion epoch, the epoch of the *B*-maximum, the maximum absolute magnitude in the *B* band, the reddening, and the distance of the SNe used for comparison throughout the paper.

SN	$t_{\rm exp}$ [MJD]	$t_{{\rm max},B}$ [MJD]	$M_{{\rm max},B}$ [mag]	$E(B-V)$ [mag]	D [Mpc]	Ref.
1987A	46849.3 (0.0)	46931.5	−14.75 (0.01)	0.19	0.05 (0.005)	1,2
1998A	50801.0 (4.0)	50890.0	−15.22 (0.20)	0.12	29.2 (2.0)	3
2000cb	51655.5 (4.1)			0.11	32.2 (8.0)	4
2006V	53747.5 (4.0)	53823.2	−16.19 (0.15)	0.03	74.5 (5.0)	5
2006au	53793.5 (9.0)	53865.0	−16.02 (0.14)	0.31	47.4 (3.2)	5
2009E	54832.0 (3.0)	54918.5	−14.53 (0.17)	0.04	29.9 (2.2)	6

References: (1) Menzies et al. (1987), (2) Catchpole et al. (1987), (3) Pastorello et al. (2005), (4) Kleiser et al. (2011), (5) Taddia et al. (2012), (6) Pastorello et al. (2012).
Note that we use the value $H_0 = 72\,{\rm km\,s^{-1}\,Mpc^{-1}}$ throughout the paper.

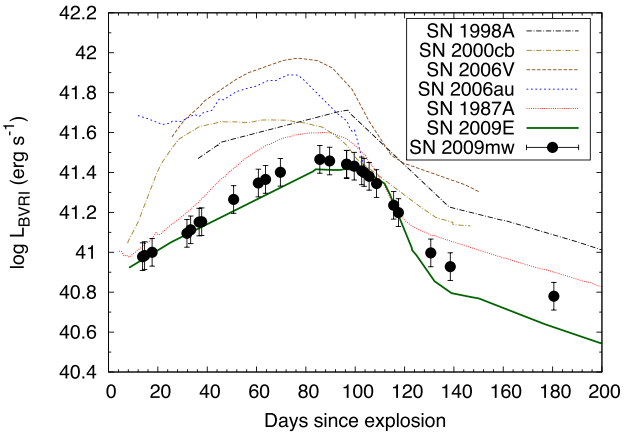

Figure 5. *BVRI* quasi-bolometric light curve of SN 2009mw and comparison with those of other 1987A-like SNe.

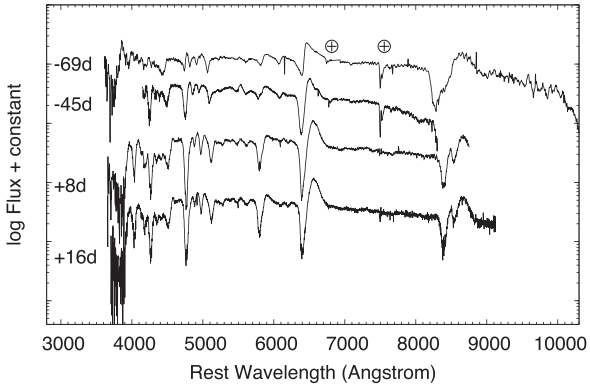

Figure 6. The spectral sequence of SN 2009mw. The positions of strong telluric features are marked with the symbol ⊕.

Table 4. Summary of the spectroscopic observations.

Date	MJD [d]	Phase[a] [d]	Instrument set-up
25/12/2009	55190.3	−69	Gemini-S+GMOS + R150
17/01/2010	55213.8	−45	Gemini-S+GMOS + R400
12/03/2010	55267.1	+8	SOAR+GOODMAN + 300
20/03/2010	55275.2	+16	du Pont+WFCCD + blue grism

[a]Relative to the epoch of the *B* maximum, i.e. MJD = 55258.8.

this can be removed by considering the expansion velocities. This is demonstrated in Fig. 11, where the sensitivity of the model to the explosion energy and the pre-SN mass (upper and lower panels, respectively) is shown. In this figure, models with different explosion energies ($E = 0.5$, 1 and 1.5 foe) and masses ($M = 15$, 19 and 22 $M_\odot$) are presented. We kept the other parameters identical to those of model M19R30E1Ni062. As shown, changing the pre-SN mass has only a small effect on the resulting velocity; it is the explosion energy that mainly regulates the photospheric velocity evolution. After setting the energy from this comparison, we varied the rest of the parameters until we found the best model to describe the observed evolution. We also found that changing the progenitor radius mainly affects the early phase of the light curve, while the ^{56}Ni mass determines the tail luminosity.

The parameters of some of the other 1987A-like SNe were determined with similar techniques. Table 5 summarizes these results. It shows that the progenitors of these objects are all compact stars, with a progenitor radius less than 100 $R_\odot$. The ejecta mass is close to 20 $M_\odot$ in all cases (although one of the models for SN 1987A found smaller values). The variation of the explosion energy is in the range of a few foe, and the nickel mass changes in the range between 0.04 and 0.13 $M_\odot$.

5 HOST ENVIRONMENT

Taddia et al. (2013) studied the environments of 1987A-like SNe and found that these objects are located either in the outer parts of bright, metal-rich galaxies or in faint, metal-poor hosts, and that on average these SNe emerge from populations with a slightly lower metallicity than that of the hosts of normal SNe II-P.

The host galaxy of SN 2009mw, ESO 499-G005, is a type SAB(s)c galaxy, with an absolute brightness of $M_B = -19.7$ mag. The SN is located in the outskirts of the galaxy (see Fig. 1), and the ratio between its deprojected position and r_{25} is $d_{SN}/r_{25} = 1.4$. We were able to extract a spectrum of an H II region close to the position of the SN from the spectrum taken with the du Pont telescope (Section 3). Using the relationships in Marino et al. (2013), we determined the oxygen abundance (12 + log (O/H)) as $N2 = 8.39 \pm 0.05$ dex (note that the systematic error of the diagnostic is 0.16 dex). As part of a project to determine the metallicity of parent populations of SNe, a VLT+FORS2 spectrum was taken of this galaxy, because it hosts another SN, namely SN 2008H (Anderson et al., in preparation). SN 2008H was located at the centre of the galaxy, corresponding to the position where the slit was placed. We were able to extract spectra at several positions along the slit and used the relationships in Marino et al. (2013) to determine the oxygen abundance. The derived metallicity is solar-like close to the centre of the galaxy and decreases along the deprojected distance from it. None of our measurements extends as far as the deprojected distance of SN 2009mw, but by extrapolating the gradient we can estimate the oxygen abundance at the distance of SN 2009mw as $N2 = 8.32 \pm 0.08$ dex, which is a subsolar value (see Fig. 12).

6 DISCUSSION

In this paper we have presented optical photometry and spectroscopy for SN 2009mw. This SN belongs to the small subgroup of 1987A-like SNe, which are Type II SNe characterized by a light curve that keeps rising for about 3 months after explosion. The current sample of 1987A-like SNe is very small, a result of the fact that they are intrinsically rare. To date, data of fewer than 18 objects have been published, and only a few of them have multiband photometric and spectroscopic data available.

We obtained a photometric follow-up of SN 2009mw using *BVRI* and $g'r'i'z'$ bands. On comparing the shape of the light curves with those of SNe 1987A, 1998A, 2006V, 2006au and 2009E we found that they are remarkably similar, while SN 2000cb has a light curve that is quite different: the slow brightening and late maximum in the *B* band is missing. The colour of SN 2009mw is bluer than that of SNe 1987A and 2000cb, and slightly redder than that of SNe 2006V and 2006au, more like that of SNe 2009E and 1998A. The absolute brightness of SN 2009mw is close to that of SNe 1987A and 2009E and fainter than that of SNe 1998A, 2000cb, 2006V and 2006au.

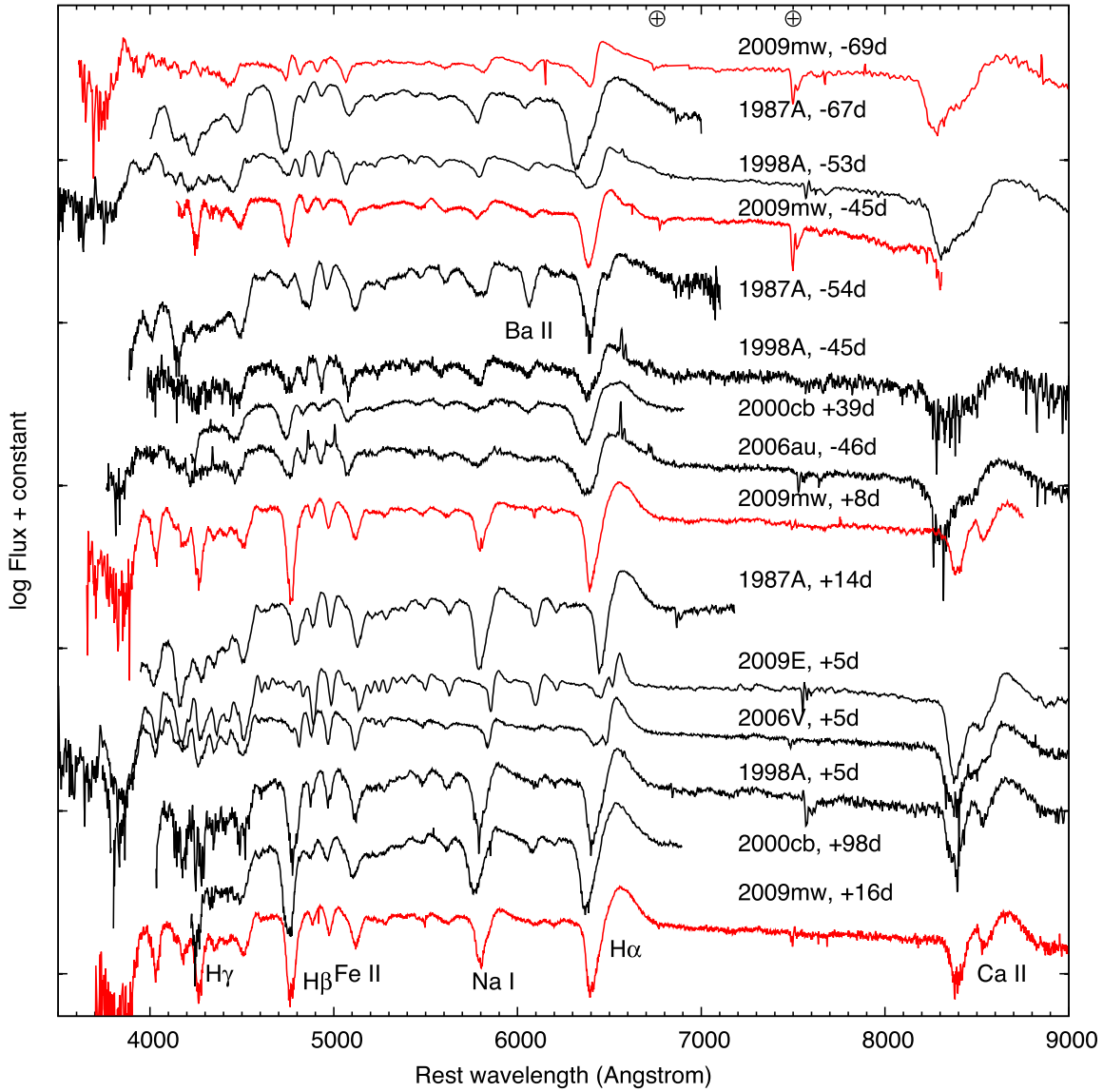

Figure 7. Comparison of the spectra of SN 2009mw with those of other 1987A-like SNe, namely SNe 1987A (Pun et al. 1995), 1998A (Pastorello et al. 2005), 2000cb (Kleiser et al. 2011), 2006V, 2006au (Taddia et al. 2012) and 2009E (Pastorello et al. 2012).

The spectra of 1987A-like SNe are similar to those of SNe II-P. The spectra of the objects in our sample evolve similarly, showing variations mostly in the strengths of the Ba II and H β lines. In this respect, the spectra of SN 2009mw are more akin to those of SNe 1998A and 2006au.

We estimated the physical properties of the progenitor and the explosion through hydrodynamical modelling, yielding an explosion energy of 1 foe, a pre-SN mass of 19 $M_{\odot}$, a progenitor radius of 30 $R_{\odot}$, and a ^{56}Ni mass of 0.062 $M_{\odot}$. These values are similar to those obtained for SN 1987A, indicating that the progenitor of SN 2009mw was a blue supergiant star, as is the case for SN 1987A. The physical parameters of several 1987A-like SNe have been estimated through modelling, and the value obtained suggest that all SNe have compact progenitors.

We examined the metallicity of the host environment of SN 2009mw and found a subsolar value for the oxygen abundance, in accordance with the findings of Taddia et al. (2013), namely that 1987A-like SNe emerge from environments with a slightly lower metallicty than those of SNe II-P.

Our comparison of SN 2009mw with other 1987A-like SNe shows that, while some of their parameters show differences, others such as their spectra, progenitors and environments are quite similar. We need a larger sample of these objects in order to understand why, for example, the light curves of SNe 2000cb and 2004ek stand out so much while their progenitors are similar to those of the rest. 1987A-like SNe seem to emerge from BSG stars located in environments with a slightly subsolar metallicity, although the processes that produce and explode these stars are still debated.

ACKNOWLEDGEMENTS

We thank N. Morrell and the Carnegie Supernova Project (CSP) for the spectrum of SN 2009mw taken with the du Pont telescope. We thank the referee for useful comments that helped to improve this paper.

KT was supported by CONICYT through the FONDECYT grant 3150473. KT, GP and MH received support from the Ministry of Economy, Development, and Tourism's Millennium Science

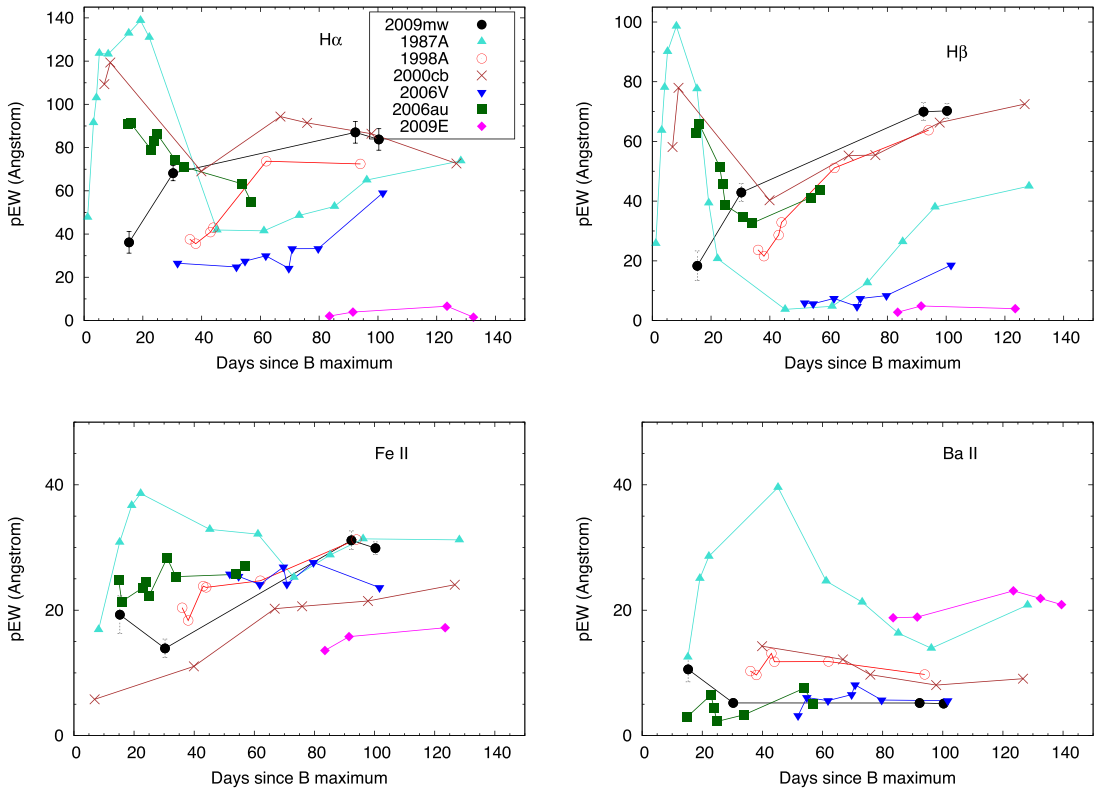

Figure 8. Pseudo-equivalent widths of the absorption components of Hα (top left panel), Hβ (top right panel), Fe II λ5169 (bottom left panel) and Ba II λ6142 features for several 1987A-like SNe, compared with those of SN 2009mw.

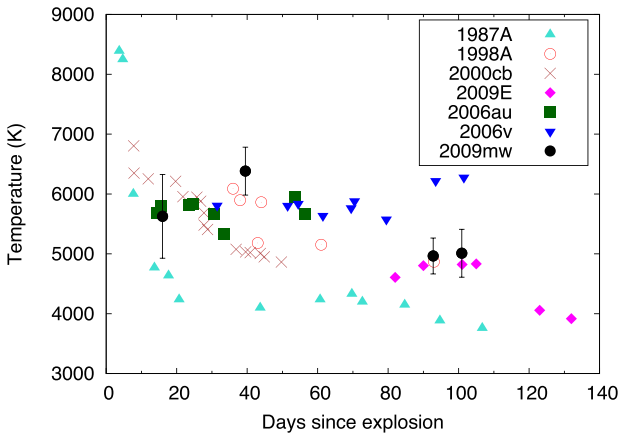

Figure 9. The evolution of the temperature of SN 2009mw compared with that of other 1987A-like SNe. The temperatures were measured by fitting blackbody curves to the spectra, except for SN 2000cb. The spectrum of this object is not flux-calibrated, and therefore the photometric spectral energy distribution was fitted with a blackbody curve.

Initiative through grant IC12009, awarded to the Millennium Institute of Astrophysics, MAS. MS gratefully acknowledges support from the Danish Agency for Science and Technology and Innovation realized through a Sapere Aude Level 2 grant.

The results are based on observations obtained at the Gemini Observatory under the program ID GS-2009B-Q-9. The Gemini Observatory is operated by the Association of Universities for

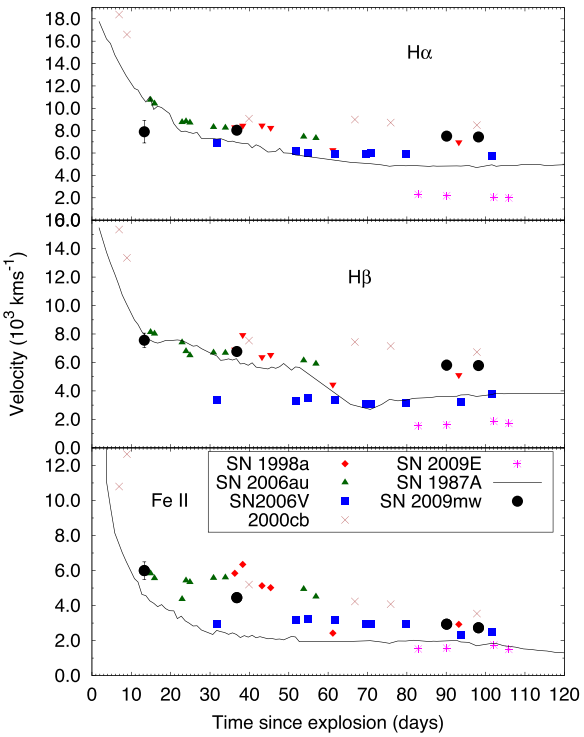

Figure 10. The expansion velocities of SN 2009mw (black circles) compared with those of other 1987A-like SNe, measured from the Doppler shift of the absorption minima of the H α (top), H β (middle) and Fe II λ5169 (bottom) features.

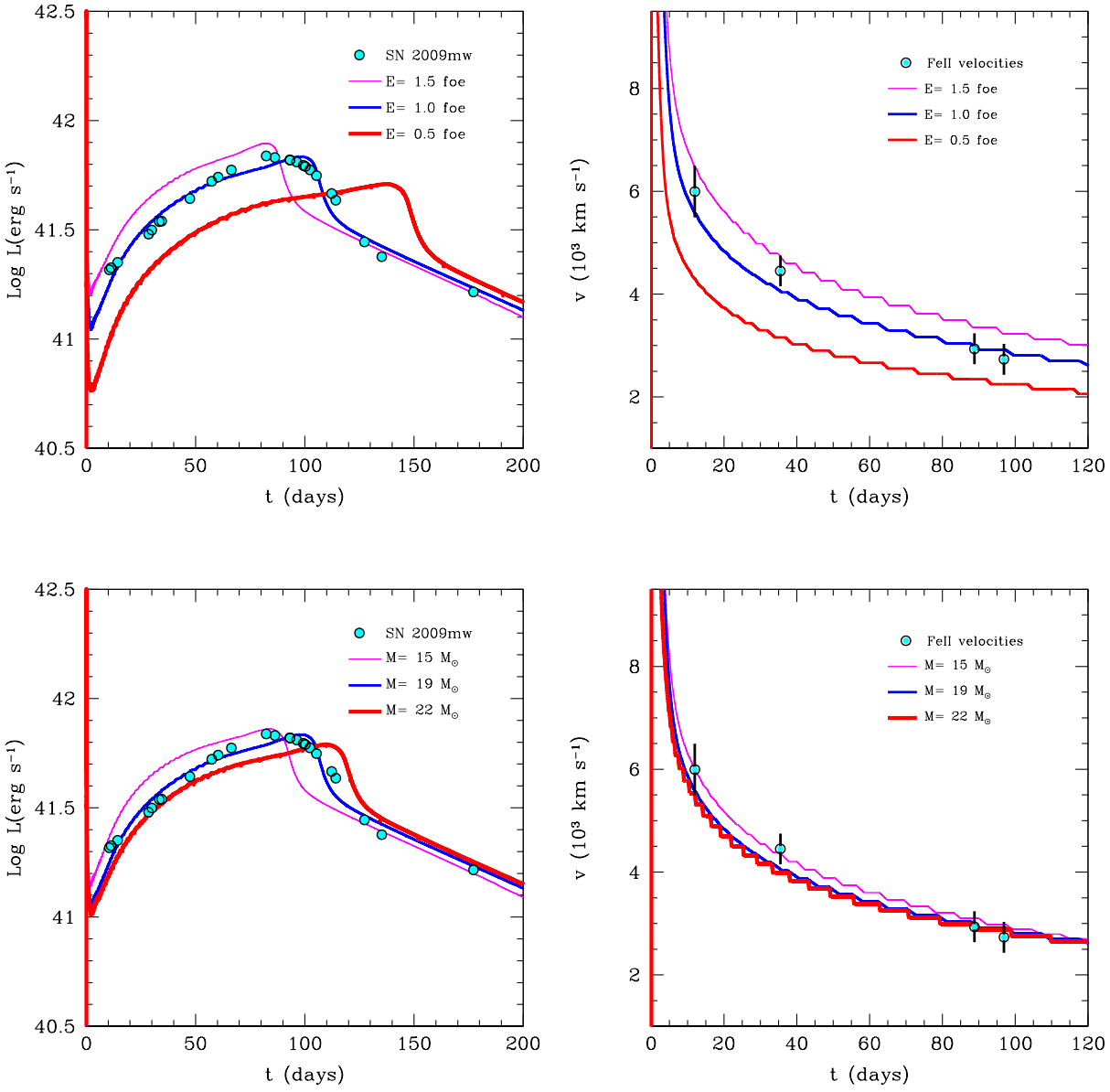

Figure 11. The bolometric luminosity (left panels) and the photospheric velocity (right panels) of SN 2009mw (circles) compared with hydrodynamical models with different parameters. The blue line shown in each panel corresponds to the best-fitting model, M19R30E1Ni062. The upper panels demonstrate the change of the model curves if we keep all parameters the same except for the explosion energy, while the lower panels show the models with different ejecta mass.

Research in Astronomy, Inc., under a cooperative agreement with the NSF on behalf of the Gemini partnership: the National Science Foundation (United States), the National Research Council (Canada), CONICYT (Chile), the Australian Research Council (Australia), Ministério da Ciência, Tecnologia e Inovação (Brazil) and Ministerio de Ciencia, Tecnología e Innovación Productiva (Argentina).

The spectra of SNe 1987A, 1998A and 2009E were downloaded from WISeREP (Weizmann Interactive Supernova data REPository, http://wiserep.weizmann.ac.il/ Yaron & Gal-Yam 2012). This research has made use of the NASA/IPAC Extragalactic Database (NED), which is operated by the Jet Propulsion Laboratory, California Institute of Technology, under contract with the National Aeronautics and Space Administration.

Table 5. Comparison of the physical parameters of the progenitor and explosion of 1987A-like SNe. The table is ordered by the brightness of the SNe, the faintest one being at the top.

SN	E [foe]	$M_{\rm ejecta}$ [$M_\odot$]	R [$R_\odot$]	^{56}Ni [$M_\odot$]	Ref.
2009E	0.6	19.0	100	0.040	1
2009mw	1.0	17.5	30	0.062	This paper
1987A	1.1	11.8	33	0.078	2
1987A	1.6	18.0	72	0.075	3
2000cb	4.4	22.3	35	0.083	4
1998A	5.6	22.0	$\leq$86	0.11	3
2006au	3.2	19.3	90	$\leq$0.073	2
2006V	2.4	17.0	75	0.127	2

References: (1) Pastorello et al. (2012), (2) Taddia et al. (2012), (3) Pastorello et al. (2005), (4) Utrobin & Chugai (2011).
Note that Pastorello et al. (2005) used the semi-analytic code of Zampieri et al. (2003) to obtain the parameters of SNe 1987A and 1998A; Pastorello et al. (2012) applied the radiation-hydrodynamics code of Pumo, Zampieri & Turatto (2010) and Pumo & Zampieri (2011); Taddia et al. (2012) used the semi-analytic model of Imshennik & Popov (1992); and Utrobin & Chugai (2011) used their own hydrodynamical model.

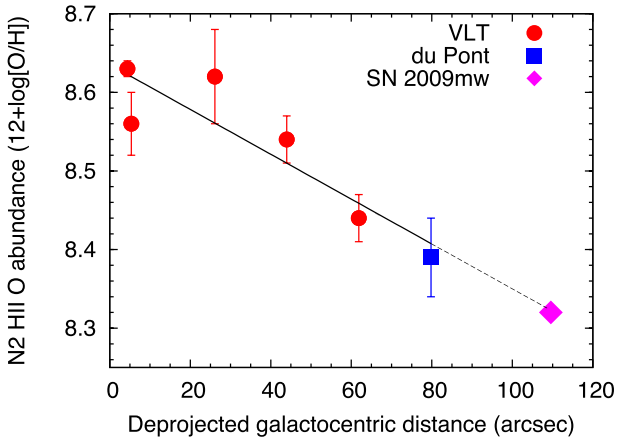

Figure 12. Using multiple measurements at various deprojected distances, we estimated the oxygen abundance at the position of SN 2009mw through extrapolation. We used a long-slit spectrum taken by Anderson et al. (in preparation) with Very Large Telescope (VLT) to extract spectra of several H II regions (red circles), as well as our spectrum of SN 2009mw taken with the du Pont telescope, to take measurements close to the site of the SN (blue square). The extrapolation yielded $N2 = 8.32 \pm 0.08$ dex, a subsolar value for the position of SN 2009mw (magenta diamond).

REFERENCES

Anderson J. P., Gutiérrez C. P., Dessart L., 2016, A&A, 589, A110
Arcavi I., 2012, in Death of Massive Stars: Supernovae and Gamma-Ray Bursts. Cambridge Univ. Press, Cambridge, p. 34
Arnett W. D., Bahcall J. N., Kirshner R. P., Woosley S. E., 1989, ARA&A, 27, 629
Bersten M. C., Benvenuto O., Hamuy M., 2011, ApJ, 729, 61
Catchpole R. M. et al., 1987, MNRAS, 229, 15
Catchpole R. M. et al., 1988, MNRAS, 231, 75
Imshennik V. S., Popov D. V., 1992, Astron. Zh., 69, 497
Jordi K., Grebel E. K., Ammon K., 2006, A&A, 460, 339
Kelly P. L. et al., 2015, preprint (arXiv:1512.09093)
Kleiser I. K. W. et al., 2011, MNRAS, 415, 372
Landolt A. U., 1992, AJ, 104, 340
Landolt A. U., Uomoto A. K., 2007, AJ, 133, 768
Lyubimkov L. S., 1991, Astron. Zh., 68, 969
Marino R. A. et al., 2013, A&A, 559, A114
Maza J. et al., 2009, Cent. Bur. Elect. Teleg., 2094, 1
Menzies J. W. et al., 1987, MNRAS, 227, 39
Pastorello A. et al., 2005, MNRAS, 360, 950
Pastorello A. et al., 2012, A&A, 537, A141
Pignata G. et al., 2009, in Giobbi G., Tornambe A., Raimondo G., Limongi M., Antonelli L. A., Menci N., Brocato E., eds, AIP Conf. Ser. Vol. 1111, Probing Stellar Populations out to the Distant Universe. AIP, New York, p. 551
Pumo M. L., Zampieri L., 2011, ApJ, 741, 41
Pumo M. L., Zampieri L., Turatto M., 2010, MSAIS, 14, 123
Pun C. S. J. et al., 1995, ApJS, 99, 223
Schlafly E. F., Finkbeiner D. P., 2011, ApJ, 737, 103
Smith J. A. et al., 2002, AJ, 123, 2121
Springob C. M., Masters K. L., Haynes M. P., Giovanelli R., Marinoni C., 2009, ApJS, 182, 474
Taddia F. et al., 2012, A&A, 537, A140
Taddia F. et al., 2013, A&A, 558, A143
Taddia F. et al., 2016, A&A, 588, A5
Takáts K. et al., 2014, MNRAS, 438, 368
Theureau G., Hanski M. O., Coudreau N., Hallet N., Martin J.-M., 2007, A&A, 465, 71
Turatto M. et al., 1998, ApJ, 498, L129
Utrobin V. P., Chugai N. N., 2011, A&A, 532, A100
Willick J. A., Courteau S., Faber S. M., Burstein D., Dekel A., Strauss M. A., 1997, ApJS, 109, 333
Yaron O., Gal-Yam A., 2012, PASP, 124, 668
Zampieri L., Pastorello A., Turatto M., Cappellaro E., Benetti S., Altavilla G., Mazzali P., Hamuy M., 2003, MNRAS, 338, 711

This paper has been typeset from a TEX/LATEX file prepared by the author.